Density-dependent intersubband absorption in strongly disordered systems

R. N. Riemann, C. Metzner, and G. H. Döhler
Institut für Technische Physik I, Universität Erlangen, Erwin-Rommel-Strasse-1, D91058 Erlangen, Germany
(Received 24 August 2001; published 19 February 2002)

We study theoretically the intersubband (IS) absorption spectrum of electrons in a center-doped quantum well (QW) as a function of the carrier density. Besides the subband quantization in z direction, the wave functions of the electrons, being directly exposed to the charged dopands, become disorder localized in the layer plane. For each set of random impurity configurations, the corresponding spectrum of quantum states is computed with a self-consistent density-functional approach, thus, taking into account the disorder and nonlinear static screening effects in a realistic way. On the basis of these effective single-particle states, we then include dynamic many-body effects (depolarization and dynamic exchange corrections) by applying and extending our recently developed theory of resonant screening in the localization regime. We analyze the relevance of the various many-body effects and find that at higher electron densities the direct static Hartree and the depolarization contributions dominate over the exchange effects. Dynamic Coulomb interactions qualitatively change the IS absorption spectrum of the statically screened electron gas, however, do not lead to a spectral narrowing in this system. A small variation of the δn-layer position within the QW affects the relative disorder strength of the two subbands and causes dramatic changes of the spectral shape and width. Our model and results are suitable for a direct comparison with experimental data.

DOI: 10.1103/PhysRevB.65.115304 PACS number(s): 73.21.−b, 78.20.Bh, 71.23.An

I. INTRODUCTION

Intersubband (IS) transitions in semiconductor quantum wells (QW) have been successfully utilized in a number of optoelectronic devices, like photodetectors,[1] modulators,[2] and lasers.[3,4] At the same time, IS processes remain in the focus of fundamental semiconductor physics, mainly due to the pronounced effect of many-body interactions on the absorption spectrum.

It is well established now that the IS resonance is a collective phenomenon of the quantized conduction subband electrons, leading to a strong, density-dependent shift of the absorption peak with respect to the single-particle IS separation.[5] Theoretically, this change of the peak position is explained by the depolarization effect, which leads to a strong blueshift with increasing density, and an excitonic correction, which produces a small redshift and dominates at low densities. Numerous experimental investigations[6–11] suggest that the present standard theory of IS absorption is in quantitative agreement with the measured absorption data, although the interpretation is often complicated by simultaneous drastic changes of the band structure as the electron density is varied.

Another long-standing problem of IS physics is the observed finite spectral width,[12–21] which is determined by a complex interplay of inhomogeneous broadening mechanisms, such as well-width fluctuations or doping-induced potential flucuations, homogeneous broadening effects, such as electron-electron scattering or short-scale interface roughness, and the collective phenomena, which tend to concentrate the distributed oscillator strength into a narrow resonance line.

While from an application point of view it is desirable to keep disorder, and thus the absorption linewidth, as small as possible, for a fundamental understanding of the underlying physics it can be more profitable to study the opposite extreme: the regime of strong disorder. When the electrons are exposed to sufficiently strong potential fluctuations, as they easily come about by closeby charged impurities, they become in-plane localized and cannot be described any longer by the usual 2D theory based on lateral translation symmetry.

It has been shown in Ref. 22 that, despite of this dramatic structural change of the electron gas, the IS spectrum in modulation-doped systems shows only a slight broadening of the absorption line (compared to the ''ordered'' case without potential fluctuations). This insensitivity is due to a tight correlation between the subbands: The edges $\epsilon_i(\vec{r})$ of the different subbands i are fluctuating heavily when viewed as a function of the lateral position $\vec{r}$, but they vary almost ''in parallel.'' For this reason, the random arrays of localized electron states (natural quantum dots) formed in the ground and first excited subband are very similar and IS absorption takes place in the form of transitions between ''correlated pairs'' of localized states (compare Fig. 1).

With respect to the external light field, each of these localized two-level systems forms an elementary oscillator with its own resonance line position. The far-field absorption spectrum simply reflects the probability distribution of the individual oscillator transition energies. In systems with almost perfect IS correlations (modulation-doped QW's), this distribution is narrow, but it becomes broader in center-doped QW's, where the ground subband is fluctuating stronger than the first excited one.

In the above picture, electron-electron interactions are not yet included. How do electrons populate the random potential profile and to which extent does this screen out the fluctuations? And how do the spatially distributed localized oscillators, under IS excitation, affect each other by long-range dynamic Coulomb interactions?

In Ref. 23, different static screening theories have been compared and applied to the case of a strongly disorded electron gas. It has been shown that in the nonlinear screening

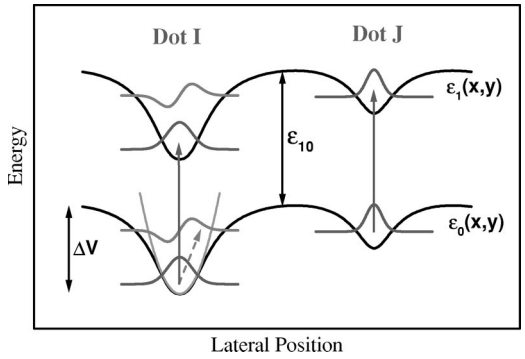

FIG. 1. Schematic showing the correlated fluctuations of the subband edges ϵ_0 and ϵ_1 in a disordered quasi-2D system and the formation of natural two-level quantum dots.

regime, corresponding to low-electron and high-impurity concentrations, the familiar and convenient random phase approximation is not applicable. Instead of treating many-body effects with a perturbative theory, it is more appropriate to view the problem as an electronic-structure calculation of a complex ''random molecule'' and, correspondingly, density-functional methods should be applied. The effect of static screening on the IS absorption spectrum has been theoretically investigated in Ref. 24.

The problem of dynamic electron-electron coupling in localized random systems has been addressed in Refs. 25,26. In this paper, an idealized model system was investigated, in which the fluctuating lateral potential landscape was approximated by a random array of rotationally symmetric, parabolic potential minima. The single-particle absorption spectrum of the correponding oscillator ensemble was artificially set to a box distribution. For this case it was found that with increasing electron density, collective phase-locking effects between the Coulomb-coupled oscillators lead to a gradual narrowing of the absorption spectrum and to a depolarization shift. The conclusion was that, even if the single-particle absorption spectrum is broad in a system with strong disorder and weak IS correlations, the actual spectrum observed at fixed carrier concentration may be narrow and of Lorentzian shape, due to the dynamic screening.

In the meantime, first experimental investigations have been conducted to elucidate the problem of the collective resonance in the localization regime, which, at least qualitatively, seem to support this theoretical picture. Pusep and co-workers[27,28] studied the plasma response of electrons in disordered superlattices, while Yakimov *et al.*[29] analyzed the depolarization shift of the interlevel resonance in a dense array of quantum dots.

Very recently (and more directly related to our present problem), Luin *et al.*[30] measured, as a function of carrier density $n^{(2)}$, the peak position and linewidth of the IS resonance in a QW, which was embedded into a field-effect transistor (FET) structure. Interestingly, in the limit of low-electron concentrations they observed a pronounced gradual line broadening, provided the temperature was kept below a certain threshold. Simultaneously, the measured absorption peak position started to deviate from the theoretical density dependence, calculated with a model that included static and dynamic many-body effects as well as the nonparabolicity of the subbands, but neglected disorder. Such a broadening and nonstandard peak shift would indeed be expected in the density regime where the strength of the many-body interactions [roughly given by the depolarization shift $\Delta E_{dep}(n^{(2)})$ in a homogeneous two-dimensional (2D) electron gas of equal density] falls below the disorder-induced width ΔE_{dis} of the single-particle spectrum.

However, in their modulation-doped QW, the disorder was mainly due to interface roughness, which produces only relatively weak localization effects. Therefore, at higher densities (or low densities and higher temperatures) a significant fraction of the carriers in the ground subband is probably occupying delocalized quantum states. Furthermore, since the electric field in the FET structure pushes the electrons more and more against the substrate-side interface of the QW, this increase of effective disorder may also contribute to the observed line broadening in the depletion region.

Clearly, it would be very important at the present stage to test the above theoretical predictions quantitatively by even more tailor-made experiments, avoiding as far as possible the above problems. To facilitate such a direct comparison, however, a consistent and comprehensive theory is required, which simultaneously has to account for all the relevant effects: Realistic disorder, IS correlations, static screening, and dynamic electron-electron interactions. In this paper, we present such a calculation and hope that the results will stimulate corresponding experiments.

The paper is organized as follows: The following Sec. II describes our proposed model system. Section III is devoted to our theoretical approach. In Sec. IV, we show and discuss our simulation results. Finally, in Sec.V, we present our conclusions.

II. MODEL SYSTEM

Since we are interested in the effectivity of static and dynamic screening processes, it is important that the fundamental disorder in the system is strong and the IS correlation effect relatively weak. For this reason, we place a δ-doped n layer of donor density $N_D^{(2)}$ directly into the center of a quantum well of width a. The width of the QW is chosen to produce an experimentally convenient IS separation.

For a study of many-body effects in the context of IS absorption it is essential that the electron density can be varied. In principle, a gradual depletion of the electrons in the QW can be achieved with a FET structure.[10,30] However, as already mentioned in the Introduction, in such systems the QW becomes more and more tilted as the density is reduced. This causes drastic changes of the subband wave functions and energies, which have nothing to do with (and, therefore, partly mask) the many-body effects. These side effects can be minimized in two ways.

One possibility consists in using an undoped QW and exciting the necessary carriers optically by interband excitation.[31] Then, in a continuous-wave experiment, the steady-state density is adjustable by the laser power. In a time-resolved experiment with pulsed excitation, the density automatically decays to zero by gradual recombination.

Since the number of electrons and holes is always the same in the QW, band-bending effects are very small. The drawback is, however, the presence of holes, which can affect the electronic IS resonance in various ways.

A simpler approach is to embed the δn-doped QW into the intrinsic region of a p-i-p structure and to attach selective electrical contacts[32–34] to the central δn layer and the outer p layers, respectively. (Alternatively, in order to enhance overall absorption, a p-i-δn-i-$\cdots$ superlattice could be used.) The advantage of this structure compared to the FET configuration is that the active QW maintains a local mirror symmetry with respect to its center for all electron densities. Thus, the trivial changes of the subbands due to band bending are less harmful. Also, tunneling escape of carriers out of the QW is small even in the almost depleted state. We have, therefore, chosen this latter approach for our model system. The average z-band profile of the central cell is shown for two different electron densities $n^{(2)}$ in Fig. 3. We define the filling factor $F=n^{(2)}/N_D^{(2)}$ of the QW as the density ratio between electrons and donors.

For most of our simulations we assumed a GaAs/AlAs QW with the following design parameters: $a=10$ nm, $N_D^{(2)}=4\times10^{12}$ cm^{-2} (structure A). We also performed some calculations for slightly modified systems, in which the central δn layer was replaced by two δn layers (each doped with $N_D^{(2)}/2$), located symmetrically around the QW center at a mutual distance $d=2$ nm (structure B), or $d=4$ nm (structure C).

In Sec. III, the capital letter $\vec{R}=(x,y,z)$ is a three-dimensional (3D) position vector, while $\vec{r}=(x,y)$ denotes the lateral coordinates only. An analogous convention is used for the momentum vectors.

III. THEORY

A. Statically screened band structure

We start from the 3D Schrödinger equation of an electron in the disordered QW,

$$\left(\frac{\hat{p}^2}{2m}+V^{(jel)}(z)+V^{(sc)}(z,\vec{r})\right)\psi^{(a)}(z,\vec{r})=E^{(a)}\psi^{(a)}(z,\vec{r}). \tag{1}$$

Here, $V^{(jel)}(z)$ is the average (jellium model) band profile in z direction and $V^{(sc)}(z,\vec{r})$ is the self-consistent (statically screened) fluctuation potential, resulting from the Coulomb potentials of the charged donors, which are located at random positions within the plane of the δn layer. Note that by definition, the lateral ($\vec{r}$) average over $V^{(sc)}(z,\vec{r})$ is zero for all z.

In general, the 3D wave function can be expanded into longitudinal (subband) modes $f_j(z)$ and lateral factors $g_j^{(a)}(\vec{r})$,[35]

$$\psi^{(a)}(z,\vec{r})=\sum_j f_j(z)g_j^{(a)}(\vec{r}), \tag{2}$$

which accounts for subband mixing induced by the nonseparable fluctuation potential $V^{(sc)}(z,\vec{r})$. In our case the wave functions appear in form of more or less strongly correlated groups, as discussed in the Introduction and schematically depicted in Fig. 1. To emphasize this structure, we assign a large index I to each group and replace the general index (a) by a superscript (I) and a subscript j. One member of group I belongs (almost) completely to the ground subband $j=0$, another to the first excited subband $j=1$. The corresponding lateral wave functions $g_0^{(I)}(\vec{r})$ and $g_1^{(I)}(\vec{r})$ are usually very similar.

For simplicity, we from now on totally *neglect subband-mixing effects* and write the member functions of each correlated group I in a factorized form

$$\psi_j^{(I)}(z,\vec{r})=f_j(z)g_j^{(I)}(\vec{r}). \tag{3}$$

In the following, we will be especially interested in the localized two-level oscillator formed by the states $\psi_0^{(I)}$ and $\psi_1^{(I)}$, which can be excited resonantly by the incident light field. Higher subbands can be disregarded in our system, because the oscillator strength of the transition between the ground and second excited subband is zero for symmetry reasons and the first excited subband is practically unoccupied in the linear absorption regime.

With the neglect of subband mixing, we can derive a 2D Schrödinger equation for the lateral functions $g_j^{(I)}$,

$$\left(\frac{\hat{p}^2}{2m}+V_{jj}^{(sc)}(\vec{r})\right)g_j^{(I)}(\vec{r})=(E_j^{(I)}-\epsilon_j)g_j^{(I)}(\vec{r}). \tag{4}$$

Here, ϵ_j is the undisturbed subband edge corresponding to the 1D jellium potential $V^{(jel)}(z)$ and $V_{jj}^{(sc)}(\vec{r})$ is a matrix element of the fluctuation potential, taken between the subband wave functions $f_j(z)$,

$$\begin{aligned}V_{jj}^{(sc)}(\vec{r})&=\langle f_j(z)|V^{(sc)}(z,\vec{r})|f_j(z)\rangle\\&=V_{jj}^{(imp)}(\vec{r})+V_{jj}^{(H)}(\vec{r})+V_{jj}^{(F)}(\vec{r}).\end{aligned} \tag{5}$$

This effective 2D potential consists of the bare impurity contribution $V_{jj}^{(imp)}$, the direct Hartree self-consistent field $V_{jj}^{(H)}$ and the exchange-correlation (or Fock) correction $V_{jj}^{(X)}$.

The 3D impurity potential, from which $V_{jj}^{(imp)}(\vec{r})$ is a 2D weighted average, is related via Poisson's equation to the impurity charge density,

$$\nabla^2V^{(imp)}(\vec{R})=(4\pi K_0/e)\rho_{imp}^{(3)}(\vec{R})$$

with

$$\rho_{imp}^{(3)}(\vec{R})=e\sum_K\delta(\vec{R}-\vec{R}_K)$$

and

$$K_0=e^2/4\pi\epsilon_0\epsilon_r. \tag{6}$$

Here, ϵ_r is the relative dielectric constant of the host material (GaAs). In practice, we solve this equation in k space, using

a fast Fourier transform algorithm and applying periodic boundary conditions in the lateral directions. (The typical lateral size of our simulation area is $L=100$ nm. Within this segment, the $N=L^2N_D^{(2)}$ impurities are assigned random, uncorrelated positions.)

Analogously, the Hartree potential is related to the electronic charge density,

$$\nabla^2 V^{(H)}(\vec{R})=(4\pi K_0/e)\rho^{(3)}(\vec{R})$$

with

$$\rho^{(3)}(\vec{R})=(-e)|f_0(z)|^2 n^{(2)}(\vec{r}). \tag{7}$$

Here we have made use of the fact that only the ground subband is occupied with electrons at low temperatures. The lateral 2D electron-density profile $n^{(2)}(\vec{r})$ can be expressed as a sum over all pairs I,

$$n^{(2)}(\vec{r})=\sum_I f(\Phi_n-E_0^{(I)})|g_0^{(I)}(\vec{r})|^2, \tag{8}$$

where $f()$ is the Fermi function and Φ_n the quasi-Fermilevel of the degenerate electron gas.

For the exchange-correlation correction in the local-density approximation,

$$V^{(F)}(\vec{R})=[f_x(n)]_{n=n(\vec{R})}, \tag{9}$$

we used the well-known expression of Ref. 36. For simplicity and reasons of consistency (see later), we decided to neglect the correlation part completely (we have convinced ourselves that its contribution is very small). The remaining exchange potential is simply proportional to the cube root of the local electron density. Using our factorized densities, we can derive the following formula:

$$\begin{aligned} V^{(F)}(\vec{R}) &= -a_X[\rho^{(3)}(\vec{R})/(-e)]^{1/3} \\ &= -a_X|f_0(z)|^{2/3}[n^{(2)}(\vec{r})]^{1/3} \end{aligned}$$

with

$$a_X=0.611(K_0/2a_B)(4\pi a_B^3/3)^{1/3}, \tag{10}$$

where $a_B=\hbar^2/(K_0 m)$ is the effective electronic Bohr radius.

Equations (4)–(10) have been solved iteratively, until convergence was achieved. Since in thermal equilibrium at low temperatures and for the relevant filling factors the carriers occupy the ground subband only, it was actually sufficient to restrict the time-consuming computations to the subspace $j=0$. As a result, we obtained the self-consistent 2D electron-density profile $n^{(2)}(\vec{r})$, from which all relevant quantities can be (re-)derived. In particular, we can calculate the 2D in-plane potentials $V_{jj}^{(sc)}(\vec{r})$ and, based on these potentials, we can compute the lateral wave functions $g_j^{(I)}(\vec{r})$ for all correlated pairs I (oscillators, natural dots) and for any subband j we wish.

B. The perfect correlation approximation

Although the lateral wave functions of the excited subband $j=1$ were not needed for the static density-functional calculation above, they come into play as soon as IS transitions or dynamic electron-electron interactions are considered. To reduce the numerical cost of these computations, we can make use of the fact that the lateral functions belonging to the same group I are very similar in our system.[22] This observation suggests to entirely neglect the small differences, leading to what we call the *perfect correlation approximation*. Consequently, we drop the subband index j from the lateral factors, using the functions of the ground state as representatives of the whole group (or pair),

$$g_j^{(I)}(\vec{r})\rightarrow g^{(I)}(\vec{r})=g_0^{(I)}(\vec{r}). \tag{11}$$

Note, however, that the corresponding energies $E_j^{(I)}$ *cannot* be assumed to be perfectly correlated. After all, fluctuations of the level differences $E_{10}^{(I)}=E_1^{(I)}-E_0^{(I)}$ are responsible for the disorder broadening ΔE_{dis} of the IS spectrum. Therefore, since we solve Eq. (4) only for the ground subband $j=0$, we have to compute the eigen energies of the $j=1$ states by some other means.

In the jellium model, $E_{10}^{(I)}$ would be equal to the undisturbed IS separation $\epsilon_{10}=\epsilon_1-\epsilon_0$. With potential fluctuations, each member state j of the correlated pair I is shifted by an amount $\Delta V_{jj}^{(I)}$ depending on the local potential profile, so that

$$E_{10}^{(I)}=\epsilon_{10}+(\Delta V_{11}^{(I)}-\Delta V_{00}^{(I)}). \tag{12}$$

We can approximately compute these shifts using first order perturbation theory:

$$\Delta V_{jj}^{(I)}=\langle g^{(I)}(\vec{r})|V_{jj}^{(sc)}(\vec{r})|g^{(I)}(\vec{r})\rangle. \tag{13}$$

The dipole moment μ_I of the oscillators is another important quantity. For the excitation with light polarized in the z direction it is a constant in our approximation,

$$\mu_I=ez^{(I)}=e\langle\Psi_1^{(I)}|z|\Psi_0^{(I)}\rangle=e\langle f_1|z|f_0\rangle=ez_{10}. \tag{14}$$

C. Dynamic electron-electron interactions and absorption

Besides the excitation energies $E_{10}^{(I)}$ of each oscillator and its dipole moment μ_I, we also need the dynamic Coulomb-interaction terms between I and all other oscillators J, consisting of the direct part $D^{(IJ)}$ and the exchange correction $X^{(IJ)}$. This dynamic Coulomb interaction can be viewed as a coherent excitation transfer process. Excited oscillator J (the source) performs a transition from $\Psi_1^{(J)}$ to $\Psi_0^{(J)}$ and transfers the released energy to oscillator I (the probe), which thereby becomes excited from $\Psi_0^{(I)}$ to $\Psi_1^{(I)}$.

The spatial fluctuation of 3D electron density due to the de-excitation of the source J is described by

$$\Delta n^{(J)}(\vec{R})=\Psi_0^{(J)\star}\Psi_1^{(J)}=f_0(z)f_1(z)|g^{(J)}(\vec{r})|^2. \tag{15}$$

The corresponding induced fluctuation of the direct Coulomb potential is

$$\Delta D^{(J)}(\vec{R}) = \int d^3R_J \frac{K_0}{|\vec{R}-\vec{R}_J|} \Delta n^{(J)}(\vec{R}_J). \tag{16}$$

From this potential fluctuation we immediately obtain the coupling strength between I and J by taking the matrix element between the initial and final state of the probe,

$$D^{(IJ)} = \langle \Psi_1^{(I)} | \Delta D^{(J)}(\vec{R}_I) | \Psi_0^{(I)} \rangle. \tag{17}$$

It corresponds to a dipole-dipole interaction for large distances r_{IJ} between source and probe and asymptotically decays like r_{IJ}^{-3}.

In a similar way we can calculate the fluctuation of the exchange potential induced by $\Delta n^{(J)}(\vec{R})$, by using the same local-density functional approximation as in Eq. (10),

$$\Delta X^{(J)}(\vec{R}) = \left[\frac{df_x}{dn} \right]_{n=n(\vec{R})} \Delta n^{(J)}(\vec{R}). \tag{18}$$

The strength of the dynamic exchange interaction between the two oscillators is then given by

$$X^{(IJ)} = \langle \Psi_1^{(I)} | \Delta X^{(J)}(\vec{R}_I) | \Psi_0^{(I)} \rangle. \tag{19}$$

This quantity depends on the overlap of the charge distribution of source and probe and thus decays exponentially with distance r_{IJ} in the localization regime. Due to the factorized wave functions, an efficient numerical evaluation of Eqs. (17) and (19) is possible with the help of Fourier transformation techniques.

We now define for each oscillator I a complex, frequency-dependent response function,

$$R^{(I)}(\omega) = \frac{1}{E_{10}^{(I)} - \hbar\omega - i\Gamma}, \tag{20}$$

where ω is the frequency of the incident light and parameter Γ accounts for homogeneous broadening of the resonance line (mainly determined by interface roughness with short correlation lengths and by spontaneous phonon emissions). The amplitude and phase of the oscillation can be described by a dimensionless complex variable $A^{(I)}(\omega)$, corresponding to the off-diagonal element (coherence) of the density matrix of the two-level system.

Without electron-electron interactions, this amplitude would simply be proportional to the field strength F of the light and the dipole moment μ_I, i.e.,

$$A^{(I)}(\omega) = eFz_{10}R^{(I)}(\omega). \tag{21}$$

With interactions, the oscillator amplitudes become coupled by a linear system of equations, which are readily solved numerically,

$$\sum_J [\delta_{IJ} - R^{(I)}(\omega)(D^{(IJ)} - X^{(IJ)})] A^{(J)}(\omega) = eFz_{10}R^{(I)}(\omega). \tag{22}$$

(For a detailed derivation see Ref. 25; compared to the original version, the above equation has been extended by the exchange interactions $X^{(IJ)}$.) From the amplitudes $A^{(I)}(\omega)$ we immediately obtain the absorption spectrum,

$$\alpha(\omega) \propto \omega \sum_I \mathrm{Im}\{A^{(I)}(\omega)\}. \tag{23}$$

We note that we have repeated our calculations for about 80 different impurity configurations and then averaged the resulting absorption spectra (each individual spectrum may be interpreted as a local property of the macroscopic system, which could, in principle, be measured by near-field techniques).

In the following, we will abbreviate the different many-body effects affecting the IS absorption process by the letters **H**, **F**, **D**, and **X**, corresponding, respectively, to the static **H**artree, static **F**ock, dynamic **D**epolarization and dynamic e**X**change effects.

IV. RESULTS AND DISCUSSION

A. Average band profiles of the model system

Figure 2 is a schematic band diagram of our p-i-δn-i-p-structure for different voltages applied to the selective contacts. The electron filling factor F in the QW can be tuned over almost the whole range between 0 and 1, without changing the mirror symmetry of the potential. The applied voltage U_{pn} is directly related to the difference of the quasi-Fermi levels Φ_n and Φ_p for electrons and holes, respectively.

In Figs. 3 and 4 we show, for different filling factors F, the average band profiles $V^{jel}(z)$ for the center-doped structure A and for the modified structure C. Note that in structure A the charged impurities (cusp in the potential) are located at the maximum of the probability distribution of the ground subband ($j=0$) electrons and at the node of the wave function of the electrons in the excited subband ($j=1$). There-

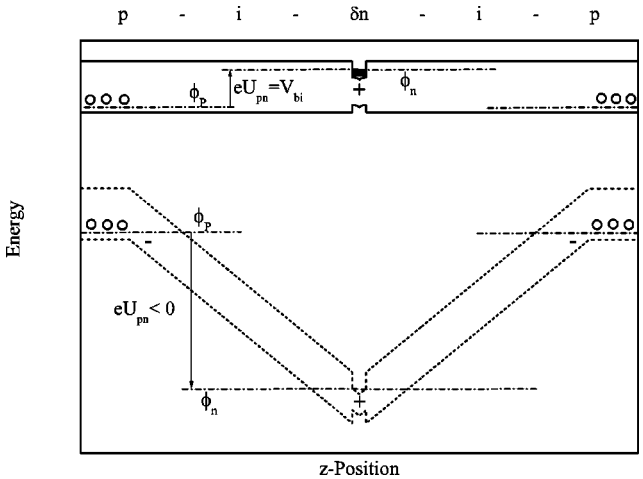

FIG. 2. Schematic band profile of a p-i-δn-i-p structure with selective contacts, for different applied voltages. The upper band diagram nearly corresponds to flat band condition (built-in voltage applied; filling factor $F=1$; full lines). In the lower diagram the QW is almost depleted of electrons (strong reverse bias applied; $F \to 0$; short dashed lines).

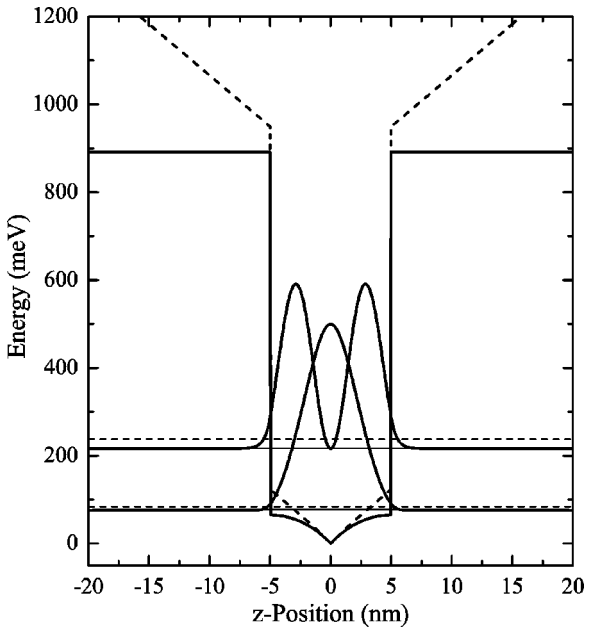

FIG. 3. Self-consistent jellium band profile and squared subband wave functions of a center-δ-doped QW (structure A) for filling factor $F=1$ (full lines) and $F=0.2$ (dashed line; wave function not shown for clarity).

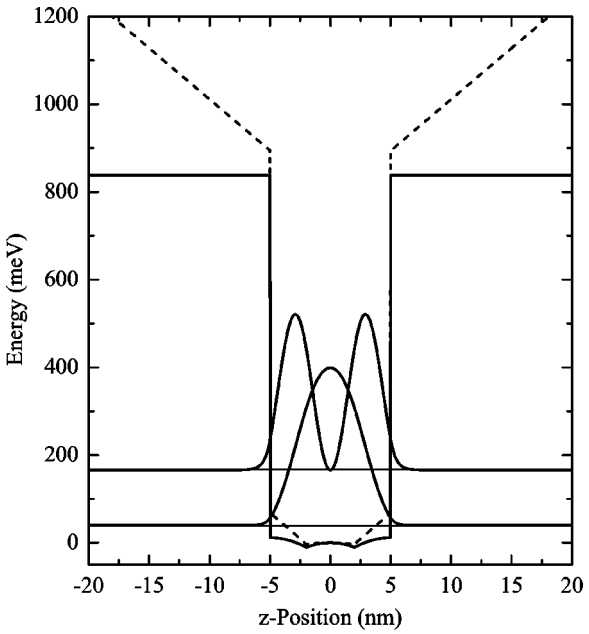

FIG. 4. Analogous to Fig. 3, however with two δ-doping layers placed symmetrically around the QW center at a mutual distance of $d=4$ nm (structure C).

fore, the subband $i=0$ will be modulated stronger by the random doping potential, leading to relatively large fluctuations of the local IS transition energy $\epsilon_1(x,y)-\epsilon_0(x,y)$ (weak IS correlations). In structure B, on the other hand, both subbands experience rather similar potential fluctuations and the IS correlations are more pronounced. As a consequence we expect, at least in the single-particle approximation, that structure A will exhibit the broadest IS absorption spectrum. Since we are interested here in the case of strong fundamental disorder, we will mainly focus on the center-doped QW in the following (structures B and C will be studied later in the context of Fig. 9).

B. In-plane potential and density profile

The mechanism of static screening of the impurity potential is visualized in Figs. 5 and 6 for a typical lateral system segment of size (100 nm).[2] In the left part of Fig. 5, we have marked the donor positions by small white circles and

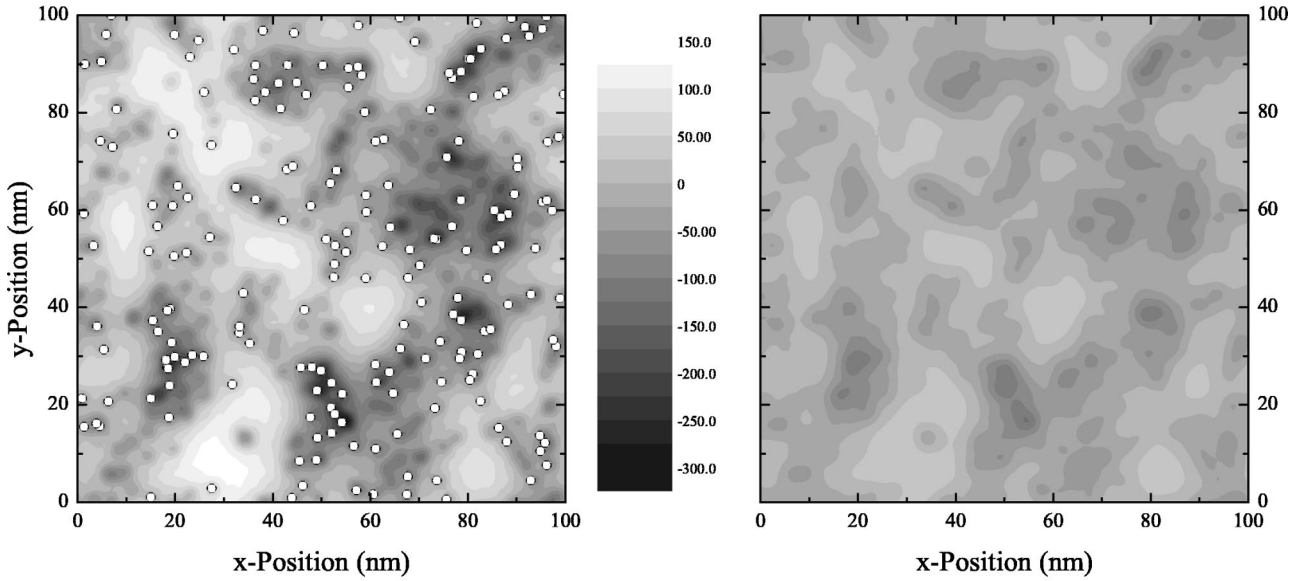

FIG. 5. Left part: Unscreened, effective impurity potential $V_{00}^{(imp)}(x,y)$ acting on the electrons in the ground subband of the center-doped QW (donor positions marked by circles). Right part: Corresponding screened, self-consistent potential $V_{00}^{(sc)}(x,y)$ for a filling factor $F=0.6$. The scale is in units of meV.

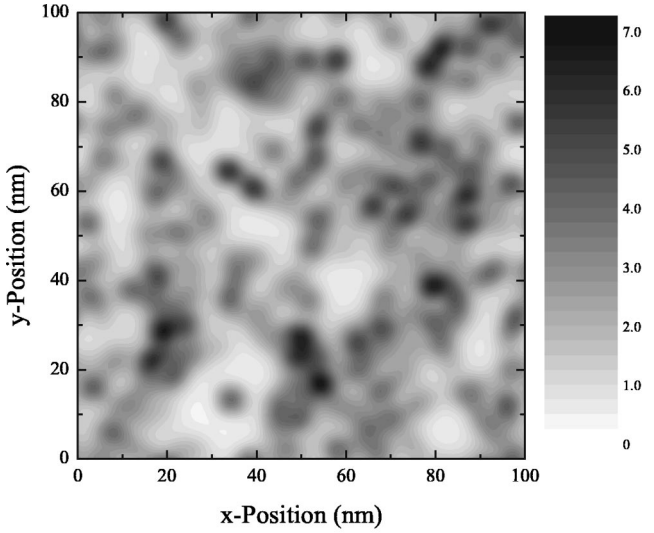

FIG. 6. Electron density distribution corresponding to the screened potential shown in the right part of Fig. 5. The scale is in units of 10^{12} cm^{-2}.

plotted on top the bare, unscreened 2D Coulomb potential $V_{00}^{(imp)}(x,y)$, which would be experienced by the ground subband electrons, if there were no many-body interactions. Note that the local potential ranges from -300 meV (minima close to statistical impurity clusters) to $+150$ meV (maxima at donor voids). In the right part we show the corresponding statically screened potential (HF approximation) for a filling factor $F=0.6$, using the same gray levels as before. It is clearly discernible how the potential landscape becomes flattened and smoothened by the action of the electrons. This effect comes about quite classically by a redistribution of the electron density (plotted in Fig. 6), in such a way that the negative carriers move to the positive donor clusters (potential minima) to compensate the local excess charge. Note that in our case of extreme disorder, there exist spatial regions with negligible carrier density besides electron ''puddles'' with peak densities of 7×10^{12} cm^{-2}.

C. Many-body effects on IS absorption

Next we turn to the IS absorption spectrum and how it is affected by the various many-body effects. In Fig. 7 we compare, for a fixed filling factor $F=0.6$, the single-particle absorption spectra (which reflect simply the distribution of oscillator resonance energies $E^{(I)}$ formed by noninteracting electrons localized in the bare impurity potential) with the spectra obtained for the approximations *H*, HF, HD, and HFDX.

The single-particle spectrum Fig. 7(a) is peaked around $\hbar\omega\approx148$ meV, which is very close to the subband separation $\epsilon_{10}=147.2$ meV in the jellium model (i.e., neglecting the disorder). However, the spectrum is very broad with a pronounced high-energy tail of at least 30 meV width, which is produced by electrons localized in the deepest potential minima (at such places, the ground-state subband is lowered much more than the excited subband). Because of this asymmetric spectral shape, the full width at half maximum (FWHM <10 meV) is no particularly useful quantity.

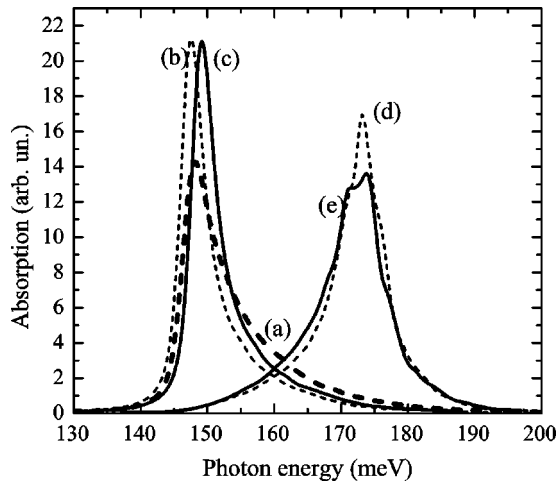

FIG. 7. Calculated IS absorption spectrum of the center-doped QW at filling factor $F=0.6$. Case (a): Without any electron-electron interaction. Case (b): Including only the static Hartree effects (*H* approximation). Case (c): Including additionally the static exchange effect (HF approximation). Case (d): Taking into account only the direct Coulomb effects, both static and dynamic (HD approximation). Case (e): Including all effects simultaneously (HFDX approximation).

If we now turn on the static Hartree interaction (*H*) in Fig. 7(b), we observe a considerable spectral narrowing and a slight redshift of the absorption peak. The narrowing, of course, reflects the smoothening of the random potential by the static electronic screening effect. Adding the exchange correction in Fig. 7(c) leaves the spectral shape almost unchanged, but causes only a small blueshift of the spectrum.

In the next step, we include both of the direct Coulomb interactions, i.e., the static Hartree (*H*) and the dynamic depolarization (*D*) contribution. Comparing the approximation *H* in Fig. 7(b) with the approximation HD in Fig. 7(d), we observe in the dynamically screened spectrum a dramatic depolarization blueshift of about 25 meV and a ''reversal'' of the peak form: Now the *low*-energy tail is much stronger pronounced. In contrast to Ref. 25, the collective resonance does not manifest itself in a line narrowing. (Actually, we even find an increase of the FWHM in our case.)

We have investigated this apparent discrepancy by studying many different model systems with qualitatively different single-particle IS absorption spectra. (In Ref. 25, a box distribution was used for the oscillator resonance energies.) Roughly speaking, it turned out that as long as the blueshifted peak of the collective resonance lies within the ''range'' of the high-energy wing of the single-particle spectrum, the collective IS absorption remains broad. It seems that the presence of even a few oscillators with resonance energies around the depolarization-shifted peak greatly disturb the collective resonance. However, if we artificially increase the dynamic electron-electron interactions sufficiently (e.g., by raising the carrier density to unrealistic values), the depolarization effect eventually blueshifts the absorption-peak to ''beyond'' the single-particle tail. At this point the spectral narrowing sets in, leading finally to a sharp collec-

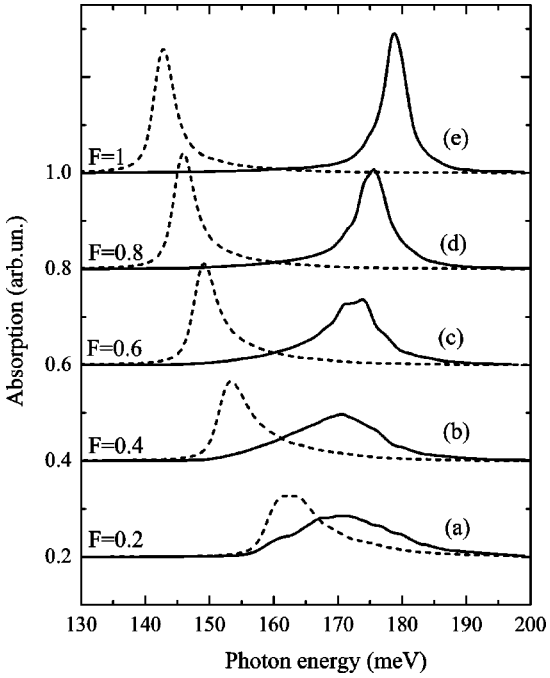

FIG. 8. IS absorption spectra of the center-doped QW as a function of the filling factor F. The dashed lines are calculated including only static many-body interactions (HF approximation), the solid lines additionally account for the dynamic Coulomb effects (HFDX approximation). The spectra have been shifted vertically for clarity. The cases (a)–(e) correspond to filling factors $F=0.2-F=1.0$ with equal increments of $\Delta F=0.2$.

tive line of Lorentzian shape and homogeneous width Γ. We will discuss this point in detail in a forthcoming paper.[37]

Finally, we also activate the static (F) and dynamic (X) exchange interactions in our simulation, arriving at the full HFDX approximation of Fig. 7(e). Obviously, the effects of F and X, when combined with H and D, are not very significant in the parameter regime shown.

The apparent fine structure on the spectrum is due to incomplete cancellation of the disorder-induced fluctuations. We note that for each individual impurity configuration, corresponding to a mesoscopic part of the whole system, the HFDX spectrum contains peaks at ''random'' photon energies and can thus be very different from the macroscopic ensemble average. These structures gradually cancel out when more and more configurations are added. However, in practice we are limited by the computation time.

D. Density dependence of IS absorption

Next, we investigate in Fig. 8 the dependence of the spectral shape on the electron density, expressed by the filling factor F. In this plot, we only include the total static model HF (dashed lines) and the full approximation HFDX (solid lines). As the filling factor rises, the HF absorption spectrum shows an almost linear redshift and a gradual peak narrowing, reflecting the increasing efficiency of the static screening of the potential fluctuations. On the other hand, the HFDX spectra, which would actually be observed in a standard IS absorption experiment, shift more and more to higher photon energies (the depolarization effect overcompensating the redshift of the static model) and, again, appear like reversed images of the corresponding static spectra.

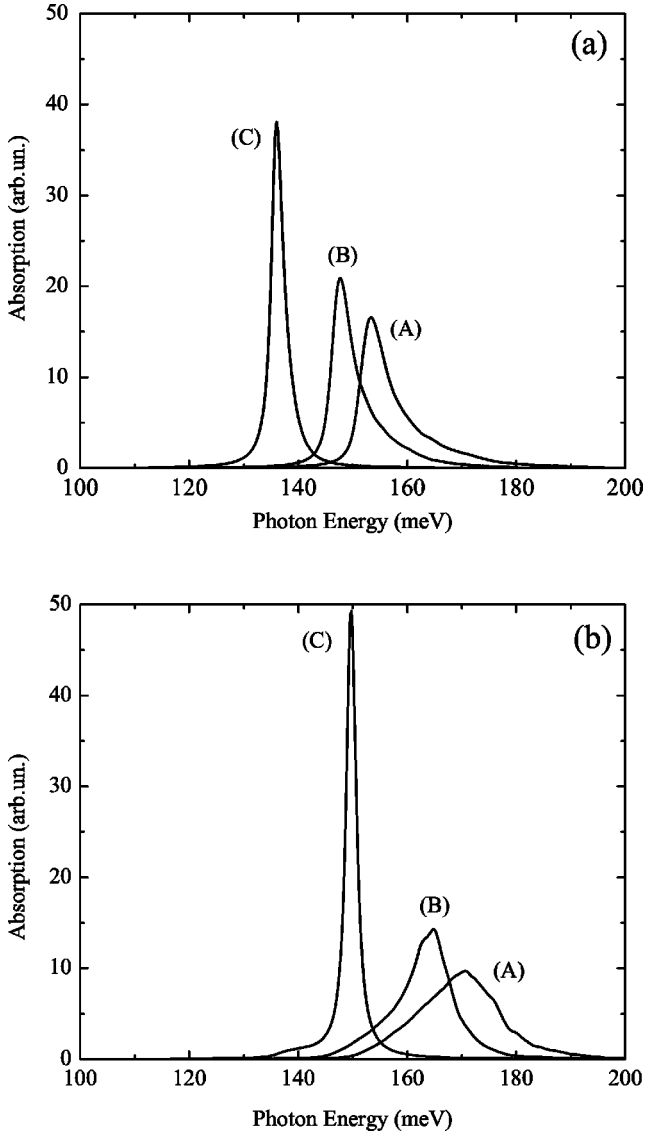

FIG. 9. Comparison of the single-particle IS absorption spectra for QWs with different δ-doping profiles at filling factor $F=0.4$: Center doped (structure A), two δ--n layers at distance $d=2$ nm (structure B) and two δ-n layers at distance $d=4$ nm (structure C, compare to Fig. 4). Part (a) corresponds to the HF approximation, part (b) to the full HFDX model.

E. Effect of doping profile

With respect to possible experiments it is illuminating to study the effect of small changes of the structural design parameters on the IS absorption spectrum. Here, the most sensitive feature is the doping profile, because it directly determines the degree of IS correlations and, thus, the width of the single-particle absorption spectrum. In Fig. 9, we compare the spectra of our three model structures A, B, C for a fixed filling factor $F=0.4$, in the static approximation [HF, part (a)] and in the full dynamic model [HFDX, part (b)].

Note that in all three cases the mirror symmetry of the jellium potential is preserved, the doping remains inside the QW, and even the total sheet density of donors is the same. The only difference is the distance d between the two sub-δn layers, which was set to $d=0$ nm (sample A), $d=2$ nm (sample B) and $d=4$ nm (sample C), respectively. The resulting difference in the HFDX absorption spectra, especially between cases (A) and (C) is surprising. In the single-particle spectrum of sample A, the high-energy wing is much more pronounced, due to the weak IS correlations. The presence of single-particle oscillators with resonance energies close to the depolarization shifted absorption peak is responsible for the great width of the HFDX spectrum.

V. CONCLUSION AND OUTLOOK

In conclusion we have presented a comprehensive numerical simulation of IS absorption in a doped QW with tunable electron concentration, which would allow a direct comparison with experiment. While the static screening effects cause a narrowing of the IS absorption spectra compared to the single-particle picture, the dynamic Coulomb interaction leads to a density-dependent depolarization blueshift and to an approximate ''reversal'' of the spectral shape. Furthermore, we demonstrated an extreme sensitivity for the position of the δ-doping layer with respect to the nodes and maxima of the subband wave functions.

At this point it appears highly desirable to test our predictions by suitably designed experiments. Besides a direct investigation of the IS absorption as a function of the filling factor (i.e., as a function of voltage applied between selective contacts to the n and p layers[32–34]), inelastic light scattering or Raman experiments would be particularly interesting. If the exciting laser is tuned to the gap between the split-off valence band and the conduction band, one can observe, besides single-particle transitions (SPT's), also charge-density excitations (CDE's, polarized spectra) and spin-density excitations (SDE's, depolarized spectra).[38–41] The CDE's are blueshifted with respect to the SPT's by dynamic depolarization (slightly compensated by exchange-correlation effects) and correspond to the IS absorption spectra. The SDE's are redshifted relatively to the SPT's only by the (small) exchange-correlation terms. Thus, our predictions concerning both kinds of spectra could be verified in a single experiment for the whole range of electron densities (except for very small values).

We note that similar experiments have been carried out previously on simple n-i-p-i superlattices.[42,43] However, in these experiments the filling factor was tunable only within a relatively narrow range by variation of the light intensity itself and the change of spectral shape could not be observed. In particular, the results were more complicated to interpret, as the IS separartion was rather close to the LO phonon energy, which implies the excitation of coupled intersubband-LO-phonon modes. These problems could be avoided with our present sample design.

ACKNOWLEDGMENTS

One of the authors (C.M.) is grateful for financial support by the German Research Foundation (DFG) and the Humboldt Foundation.

[1] B. Levine, K. Choi, C. Bethea, J. Walker, and R. Malik, Appl. Phys. Lett. **50**, 1092 (1987).
[2] N. Vodjani, B. Vinter, V. Berger, E. Bockenhoff, and E. Costard, Appl. Phys. Lett. **59**, 555 (1989).
[3] J. Faist, F. Capasso, L. Sivco, C. Sirtori, A. Hutchinson, and A. Cho, Science **264**, 553 (1994).
[4] H. C. Lui, I. W. Cheung, A. J. SpringThorpe, C. Dharma-wadana, Z. R. Wasilewski, D. J. Lockwood, and G. C. Aers, Appl. Phys. Lett. **78**, 3580 (2001).
[5] M. Helm, in *Intersubband Transitions in Quantum Wells, Physics and Device Applications I*, Semiconductors and Semimetals Vol. 62, edited by H. C. Liu and F. Capasso (Academic Press, New York, 2000).
[6] R. Sasagawa, H. Sugawara, Y. Ohno, H. Nakajima, S. Tsujino, H. Akiyama, and H. Sakaki, Appl. Phys. Lett. **72**, 719 (1998).
[7] R. J. Warburton, K. Weilhammer, J. P. Kotthaus, M. Thomas, and H. Kroemer, Phys. Rev. Lett. **80**, 2185 (1998).
[8] S. Graf, H. Sigg, K. Köhler, and W. Bächtold, Phys. Rev. Lett. **84**, 2686 (2000).
[9] H. C. Liu and A. J. SpringThorpe, Phys. Rev. B **61**, 15 629 (2000).
[10] S. Tsujino, M. Rüfenacht, H. Nakajima, T. Noda, C. Metzner, and H. Sakaki, Phys. Rev. B **62**, 1560 (2000).
[11] S. Ernst, A. R. Goni, K. Syassen, and K. Eberl, Phys. Rev. Lett. **72**, 4029 (1994).
[12] Paul von Allmen, M. Berz, F. K. Reinhart, and G. Harbeke, Semicond. Sci. Technol. **3**, 1211 (1988).
[13] T. Ando, J. Phys. Soc. Jpn. **54**, 2671 (1985).
[14] E. B. Dupont, D. Delacourt, D. Papillon, J. P. Schnell, and M. Papuchon, Appl. Phys. Lett. **60**, 2121 (1992).
[15] J. Faist, F. Capasso, C. Sirtori, D. L. Sivco, A. L. Hutchinson, Sung Nee G. Chu, and A. Y. Cho, Appl. Phys. Lett. **65**, 94 (1994).
[16] K. L. Campman, H. Schmidt, A. Imamoglu, and A. C. Gossard, Appl. Phys. Lett. **69**, 2554 (1996).
[17] J. Faist, C. Sirtori, F. Capasso, L. Pfeiffer, and K. W. West, Appl. Phys. Lett. **64**, 872 (1994).
[18] G. Beadie, W. S. Rabinovich, D. S. Katzer, and M. Goldberg, Phys. Rev. B **55**, 9731 (1997).
[19] T. Unuma, T. Takahashi, T. Noda, M. Yoshita, H. Sakaki, M. Baba, and H. Akiyama, Appl. Phys. Lett. **78**, 3448 (2001).
[20] J. B. Williams, M. S. Sherwin, K. D. Maranowski, and A. C. Gossard, Phys. Rev. Lett. **87**, 037401 (2001).
[21] C. A. Ullrich and G. Vignale, Phys. Rev. Lett. **87**, 037402 (2001).
[22] C. Metzner, M. Hofmann and G. H. Döhler, Phys. Rev. B **58**, 7188 (1998).
[23] K. Schrüfer, C. Metzner, M. Hofmann, and G. H. Döhler, Superlattices Microstruct. **21**, 223 (1997).
[24] C. Metzner, M. Hofmann, and G. H. Döhler, Superlattices Microstruct. **25**, 239 (1999).

[25] C. Metzner and G. H. Döhler, Phys. Rev. B **60**, 11 005 (1999).
[26] C. Metzner and G. H. Döhler, Physica E (Amsterdam) **7**, 718 (2000).
[27] Yu. A. Pusep, J. Phys.: Condens. Matter **12**, 3897 (2000).
[28] Yu. A. Pusep and A. J. Chiquito, J. Appl. Phys. **88**, 3093 (2000).
[29] A. I. Yakimov, A. V. Dvurechenskii, N. P. Stepina, and A. I. Nikiforov, Phys. Rev. B **62**, 9939 (2000).
[30] S. Luin, V. Pellegrini, F. Beltram, X. Marcadet, and C. Sirtori, Phys. Rev. B **64**, R041306 (2001).
[31] I. Shtrichman, C. Metzner, E. Ehrenfreund, D. Gershon, and A. C. Gossard, Phys. Rev. B **65**, 035310 (2002).
[32] G. H. Döhler, G. Hasnain, and J. N. Miller, Appl. Phys. Lett. **49**, 704 (1986).
[33] K. H. Gulden, X. Wu, J. S. Smith, P. Kiesel, A. Hoefler, M. Kneissl, P. Riel, and G. H. Doehler, Appl. Phys. Lett. **62**, 3180 (1993).
[34] We note that selective *n*- and *p*-contacts can also be achieved without the shadow mask technique by allowing lateral Ni-Ge-Au- and Au-Zn-Au layers, respectively, as described in R. Windisch, M. Kneisel, P. Kiesel, B. Knüpfer, and G. H. Döhler, IEEE Photonics Technol. Lett. **8**, 1325 (1996).
[35] In our numerical calculation we further expanded the lateral functions $g_j^{(a)}(\vec{r})$ into plane waves, $g_j^{(a)}(\vec{r})=\Sigma_{\vec{k}} A_{j\vec{k}}^{(a)} e^{i\vec{k}\vec{r}}$, using a finite lateral simulation area of linear size $L=100$ nm and periodic boundary conditions.
[36] L. Hedin and B. I. Lundqvist, J. Phys. C **4**, 2064 (1971).
[37] C. Metzner, N. Riemann, and G. H. Döhler (unpublished).
[38] P. Ruden and G. H. Döhler, Phys. Rev. B **27**, 3547 (1983).
[39] A. Pinczuk and G. Abstreiter, in *Light Scattering in Solids V*, edited by M. Cardona and G. Güntherodt (Springer-Verlag, Berlin, 1989), p. 153.
[40] A. Pinczuk, S. Schmitt-Rink, G. Danan, J. P. Valladares, L. N. Pfeiffer, and K. W. West, Phys. Rev. Lett. **63**, 1633 (1989).
[41] D. Gammon, B. V. Shanabrook, J. C. Ryan, and D. S. Katzer, Phys. Rev. B **41**, 12 311 (1990).
[42] Ch. Zeller, B. Vinter, and G. Abstreiter, Physica B & C **117**, 729 (1983).
[43] G. Fasol, P. Ruden, and K. Ploog, J. Phys. C **17**, 1395 (1984).